ELSEVIER

Polymer 43 (2002) 6853–6861

polymer

www.elsevier.com/locate/polymer

Specific interactions and miscibility of ternary blends of poly(2-vinylpyridine), poly(*N*-vinyl-2-pyrrolidone) and aliphatic dicarboxylic acid: effect of spacer length of acid

X.D. Li, S.H. Goh*

Department of Chemistry, National University of Singapore, 3 Science Drive, Singapore, Singapore 117543

Received 22 March 2002; received in revised form 26 August 2002; accepted 11 September 2002

Abstract

Fourier transform infra-red spectroscopy was used to study the specific interactions between three aliphatic dicarboxylic acids, namely succinic acid (SCA), suberic acid (SBA) and dodecanedioic acid (DDA), and two proton-accepting polymers, poly(2-vinylpyridine) (P2VPy) and poly(*N*-vinyl-2-pyrrolidone) (PVP). P2VPy interacts with the acids through hydrogen-bonding interaction as well as ionic interaction, while PVP interacts with the acids through hydrogen-bonding interaction. The intensity of interaction decreases in the order SCA > SBA > DDA, which is in the reverse order of the spacer length between two carboxylic groups of the acid. The miscibility of ternary P2VPy/PVP/acid blends was examined by differential scanning calorimetry, scanning electron microscopy and solid-state ^{13}C nuclear magnetic resonance spectroscopy. The interaction strength and the spacer length play important roles in the miscibility and phase behavior of P2VPy/PVP/acid blends. SCA interacts most strongly with P2VPy and PVP, but SBA has a better miscibilization effect due to its longer spacer. However, DDA, which has the longest spacer, is unable to miscibilize P2VPy/PVP blends.

Keywords: Ternary blends; Miscibility; Phase behavior

1. Introduction

The phase behavior and miscibility of ternary polymer blends have been extensively studied in view of their industrial importance. Most of the studies are focused on the miscibilization of two immiscible polymers by adding a third component which is miscible with both polymers [1–5]. For ternary blends consisting of three miscible binary pairs, completely miscible blends over the entire composition range [6–9] or immiscibility loops [10–13] have been observed.

The interactions between polymers and low molecular weight (LMW) compounds have received increasing attention in recent years [14,15]. Inoue et al. have made extensive studies on specific interactions between polymers and bifunctional LMW compounds [16–22]. Wu et al. have also studied the interaction between some polymers and dihydric phenols [23–25] and they found that a bifunctional hindered phenol could compatibilize immiscible chlorinated polyethylene/acrylic rubber blends [26]. We have recently reported the miscibilization of poly(2-vinylpyridine) (P2VPy) and poly(*N*-vinyl-2-pyrrolidone) (PVP) blend with some bisphenols such as bis(4-hydroxyphenyl)-methane (BHPM), Bisphenol A (BPA) and 4,4′-(1,4-phenylenediisopropylidene)bisphenol (PDIPBP) [27–29]. Kuo et al. [30] recently reported the miscibilization of immiscible PVP/poly(vinylacetate) blends by BPA. In this paper, we report the specific interactions and the miscibility in ternary blends of P2VPy, PVP and three aliphatic dicarboxylic acids, namely succinic acid (SCA, $HOOC(CH_2)_2COOH$), suberic acid (SBA, $HOOC(CH_2)_6COOH$) and dodecanedioic acid (DDA, $HOOC(CH_2)_{10}COOH$). Carboxylic acids are stronger acids than phenols, and their interactions with P2VPy and PVP are likely to be stronger, and hence the miscibility and phase behavior of the ternary blends may be affected. We also found that an improvement in the compatibilization efficiency may be achieved if the two functional moieties in the compatibilizer are separated by spacer groups [31]. The dicarboxylic acids

* Corresponding author. Tel.: +65-68742844; fax: +65-67791691.
E-mail address: chmgohsh@nus.edu.sg (S.H. Goh).

0032-3861/02/$ - see front matter
PII: S0032-3861(02)00659-6

used in this study have different spacer lengths between two carboxylic groups, and therefore the influence of varying spacer length on the miscibility and phase behavior can be studied.

2. Experimental

2.1. Materials

P2VPy (weight-average molecular weight (M_w) = 200,000 g/mol), was supplied by Scientific Polymer Products, Inc. PVP (M_w = 40,000 g/mol) was supplied by Aldrich Chemical Company, Inc. SBA was supplied by Sigma Chemical Co. SCA was supplied by Merck and DDA was supplied by Fluka Chemie GmbH. All materials were used as received without further purification.

2.2. Preparation of blends

All the blends were prepared by solution casting from ethanol (2%, w/v). To remove the residual solvent, the blends were then dried in vacuo at 60 °C for 2 weeks. The blends are denoted as (polymer)$_x$acid where x is the molar ratio of polymer repeating unit to acid for binary blends, and as (P2VPy)$_x$(PVP)$_y$(acid)$_z$ for ternary blends, where x:y:z is the molar ratio of the repeating unit of P2VPy to that of PVP and to acid.

2.3. WAXD measurements

A Siemens D5005 X-ray powder diffractometer with Cu Kα (1.54051 Å) radiation (40 kV, 40 mA) was used to record the wide-angle X-ray diffraction (WAXD) patterns of the blends at a scanning step of 0.02°/s (in 2θ). The measurements were conducted at room temperature.

2.4. Thermal analysis

Thermal analysis was carried out on a TA Instruments 2920 differential scanning calorimeter (DSC). For the glass transition temperature (T_g) measurements, the blends were heated to a temperature above the melting point of each acid using a heating rate of 20 °C/min. The samples were kept at that temperature for 3 min before being quenched to a temperature which is about 50 °C below the glass transition of each blend. The quenched samples were then re-scanned and the midpoints of the heat capacity jump in the DSC curves were taken to be the T_gs. All measurements were conducted under a nitrogen atmosphere.

2.5. FTIR characterization

Fourier transform infrared (FTIR) spectra were recorded on a Bio-Rad 165 FTIR spectrophotometer; 32 scans were signal-averaged at a resolution of 2 cm^{-1}. In view of the hygroscopic nature of the polymers, spectra were recorded at 120 °C using a SPECAC high-temperature cell, equipped with an automatic temperature controller, which was mounted in the spectrophotometer. Blend samples were prepared by dropping the ethanol solutions to KBr powder followed by drying in vacuo at 60 °C for 2 weeks. The mixtures were then ground and compressed to form disks. The KBr disks were further dried in vacuo at 60 °C for another 2 days and then stored in a desiccator.

2.6. Scanning electron microscopy

The films of samples were cryofractured in liquid nitrogen. The fracture surfaces were then sputter-coated with gold and observed with a Philips XL30 scanning electron microscope (SEM) using an accelerating voltage of 10 kV.

2.7. Solid-state CP/MAS ^{13}C NMR experiment

High-resolution solid-state ^{13}C nuclear magnetic resonance (NMR) experiments were carried out on a Bruker DRX-400 MHz NMR spectrometer operating at resonance frequencies of 100.62 and 400.13 MHz for ^{13}C and ^{1}H, respectively. The proton spin–lattice relaxation times in the rotating frame, $T_{1\rho}$(H), were determined by spin-locking method using varied spin-lock time. The proton spin–lattice relaxation times in the laboratory frame, T_1(H), were determined using an inversion-recovery sequence ($\pi-\tau-\pi/2$) followed by the CP scheme [32]. The pulse delay time was 3 s and the magic angle spinning (MAS) rate was kept at 8 kHz during the experiments.

3. Results and discussion

3.1. Specific interaction

FTIR has been used to study specific interactions [33]. In blends of P2VPy, the pyridine skeleton vibration band at 1588 cm^{-1} shifts to a higher frequency upon the formation of hydrogen bonds [34,35]. Fig. 1 shows the FTIR spectra of P2VPy/acid blends in this region. New bands develop at higher frequencies and the intensity increases with increasing acid content, demonstrating the involvement of pyridine group in specific interaction. From the intensity of the new bands, more pyridine groups in the P2VPy/SCA blends are involved in interaction than those in the P2VPy/SBA and P2VPy/DDA blends at the same 2VPy/acid molar ratio. For a better illustration, the FTIR spectra of the (P2VPy)$_1$SCA, (P2VPy)$_1$SBA and (P2VPy)$_1$DDA blends are plotted in Fig. 2. One can also find from Figs. 1 and 2 that, the shift of pyridine band in the P2VPy/SCA blends is larger than that in the P2VPy/SBA and P2VPy/DDA blends. Drago et al. [36,37] have shown that for hydroxyl-containing LMW compounds undergoing hydrogen bonding interactions,

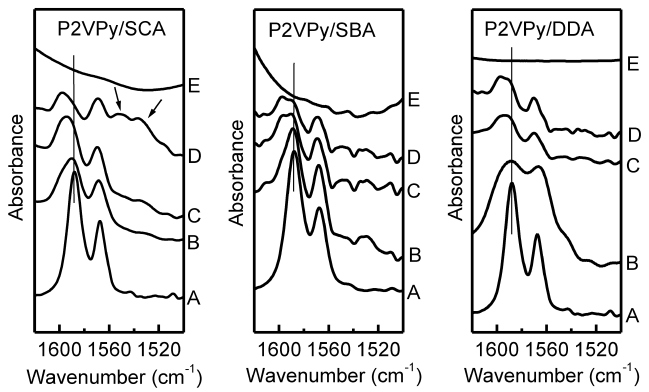

Fig. 1. FTIR spectra, recorded at 120 °C, in the pyridine region of P2VPy/carboxylic acid blends. (A) P2VPy; (B) $(P2VPy)_4$acid; (C) $(P2VPy)_2$acid; (D) $(P2VPy)_1$acid; (E) acid.

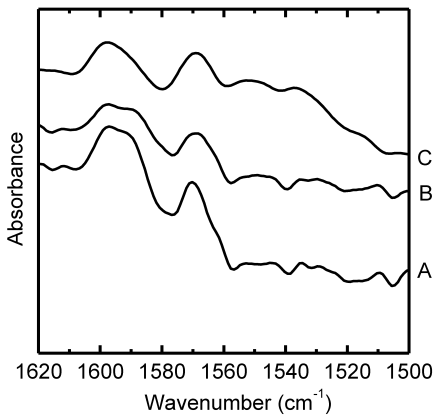

Fig. 2. FTIR spectra, recorded at 120 °C, in the pyridine region of P2VPy/carboxylic acid blends. (A) $(P2VPy)_1$DDA; (B) $(P2VPy)_1$SBA; (C) $(P2VPy)_1$SCA.

there is a linear relationship between the frequency shift of hydroxyl band and the enthalpy of mixing. Therefore, a change in frequency and intensity of a particular band as observed in the present study can be used as a measurement, at least qualitatively, for the strength of interaction. Therefore this result indicates that P2VPy interacts most strongly with SCA among the three dicarboxylic acids.

The carbonyl stretching region of the carboxylic group is also of interest to study. The carbonyl stretching band is located around 1700 cm^{-1} which is at a lower frequency than the ester carbonyl band due to the dimerization of carboxylic groups. Upon the formation of a weak to medium interaction, e.g. hydrogen bonding interaction, this band at 1700 cm^{-1} shifts to a higher frequency due to the disruption of dimerization [38], while it shifts to a lower frequency when ionic interaction occurs [39]. Fig. 3 shows the FTIR spectra of the carbonyl region of P2VPy/acid blends. High-frequency shifts of the carbonyl stretching band are observed in these blends, showing the presence of hydrogen bonding interaction. Interestingly, new bands at about 1630 cm^{-1} are observed, which are particularly intense in the P2VPy/SCA blends. As shown in Fig. 1, one can find that, new broad bands in the region of 1500–1550 cm^{-1} appear. Usually the skeleton vibration band of protonated pyridine is at about 1630 cm^{-1} and the stretching vibration band of carbonyl group of an ionized carboxylic group is between 1500 and 1600 cm^{-1}, consisting of the symmetric and antisymmetric stretching modes. Therefore, the FTIR spectra of the P2VPy/SCA blends suggest that both ionic and hydrogen-bonding interactions are present between P2VPy and SCA. The ionic interaction in the P2VPy/SBA blends is much less than that in the P2VPy/SCA blends, and becomes almost imperceptible in the P2VPy/DDA blends. In terms of ionic interaction, the interaction strength is in the order SCA > SBA > DDA.

Fig. 4 shows the FTIR spectra in the carbonyl region of PVP/carboxylic acid blends. Although the carbonyl stretching bands of PVP and the acids overlap, interactions between PVP and the carboxylic acids are still evidenced from the spectra. New carbonyl bands develop at around 1650 cm^{-1}, which is ascribed to the stretching vibration of hydrogen-bonded PVP carbonyl group. The intensity of the new vibration bands suggests that the proportion of dimerized carbonyl groups of carboxylic acids decreases upon blending with PVP. No ionized carboxylic vibration band appears in the region of 1500–1550 cm^{-1},

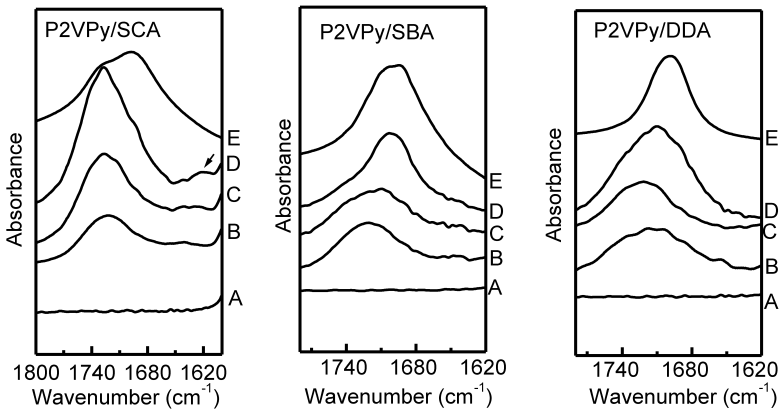

Fig. 3. FTIR spectra, recorded at 120 °C, in the carbonyl region of P2VPy/carboxylic acid blends. (A) P2VPy; (B) $(P2VPy)_4$acid; (C) $(P2VPy)_2$acid; (D) $(P2VPy)_1$acid; (E) acid.

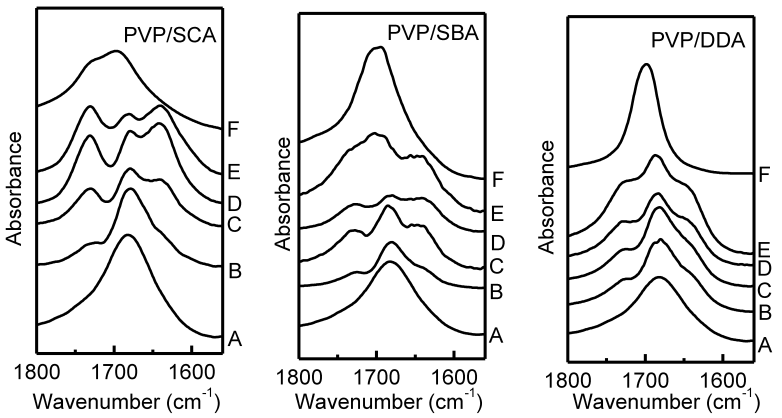

Fig. 4. FTIR spectra, recorded at 120 °C, in the carbonyl region of PVP/carboxylic acid blends. (A) PVP; (B) $(PVP)_{10}$acid; (C) $(PVP)_4$acid; (D) $(PVP)_2$acid; (E) $(PVP)_1$acid; (F) acid.

demonstrating that the interactions between PVP and the acids are essentially hydrogen-bonding interactions.

3.2. Saturation of acids in P2VPy and PVP

Fig. 5 shows the WAXD patterns of various P2VPy/SCA, P2VPy/SBA and P2VPy/DDA blends. At low acid contents, the patterns show no diffraction, indicating that the blends are amorphous. With increasing carboxylic acid content, diffraction peaks appear at different 2VPy/acid molar ratios for different acids, 1:1 for P2VPy/SCA blends, 2:1 for P2VPy/SBA blends and 4:1 for P2VPy/DDA blends. Therefore the acid crystallizes out from the amorphous phase when its content reaches a certain limit. The three acids have different saturation contents. SCA is saturated at the lowest 2VPy/carboxylic acid molar ratio while DDA is saturated at the highest 2VPy/carboxylic acid ratio.

Fig. 6 shows the WAXD patterns of various PVP/SCA, PVP/SBA and PVP/DDA blends. Similarly, as in blends with P2VPy, DDA crystallizes out from PVP at a very low content, while SCA has the highest saturation content.

3.3. Glass transitions of binary blends

Figs. 7 and 8 show the T_gs of P2VPy/acid and PVP/acid blends. The addition of dicarboxylic acids lowers the T_gs of P2VPy and PVP, demonstrating the plasticization effect of these acids. The acids disperse into the polymers and expand the space between the macromolecule chains and thus enhance their mobility and lower the T_gs. On the other hand, specific interaction between the polymer and the acid may enhance the rigidity of the polymer chain and increase its T_g. In the present case, the former factor dominates. The T_gs of P2VPy and PVP decrease dramatically upon blending with the acids and the decrease slows down at high acid contents, and finally the T_gs approach constant values. Since the polymer is saturated with the acid at a sufficiently high acid content, the compositions of the amorphous phases do not change further above the saturation limits, and therefore the T_gs of the blends do not change further.

3.4. Miscibility of ternary blends

Fig. 9 shows the FTIR spectra of ternary $(P2VPy)_1$-

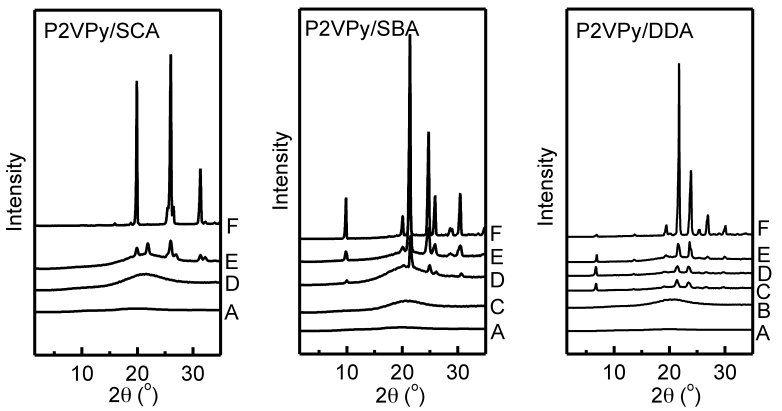

Fig. 5. WAXD patterns of various P2VPy/carboxylic acid blends. (A) P2VPy; (B) $(P2VPy)_{10}$acid; (C) $(P2VPy)_4$acid; (D) $(P2VPy)_2$acid; (E) $(P2VPy)_1$acid; (F) acid.

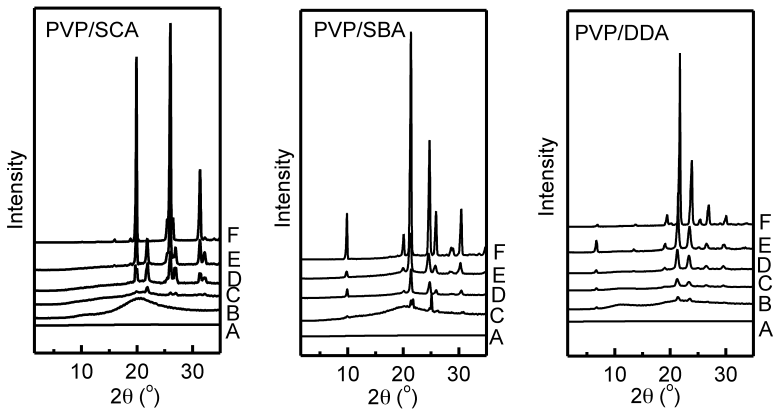

Fig. 6. WAXD patterns of various PVP/carboxylic acid blends. (A) PVP; (B) $(PVP)_{10}$acid; (C) $(PVP)_4$acid; (D) $(PVP)_2$acid; (E) $(PVP)_1$acid; (F) acid.

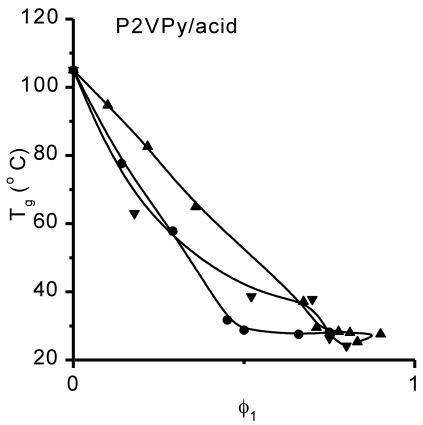

Fig. 7. T_gs of (▲) P2VPy/SCA; (●) P2VPy/SBA and (▼) P2VPy/DDA blends.

$(PVP)_1(SCA)_1$, $(P2VPy)_1(PVP)_1(SBA)_1$ and $(P2VPy)_1$-$(PVP)_1(DDA)_1$ blends. Hydrogen-bonded carbonyl stretching bands of PVP and hydrogen-bonded pyridine skeleton vibration bands are observed in these blends, demonstrating that both P2VPy and PVP interact with the acids in the ternary blends. A pyridine group of P2VPy and a carbonyl group of PVP may be linked either by a single acid molecule (Scheme 1) or by an associated acid chain (Scheme 2). In addition, there is also 'ineffective' interaction in which the two acid groups interact with the same kind of polymer.

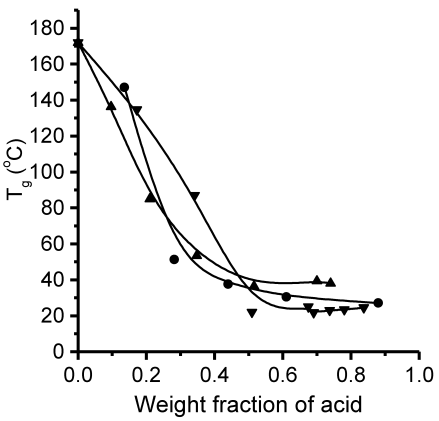

Fig. 8. T_gs of (▲) PVP/SCA; (●) PVP/SBA and (▼) PVP/DDA blends.

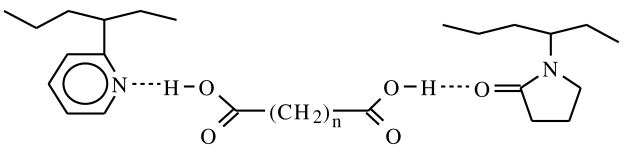

Scheme 1.

Figs. 10–12 show the DSC curves of various P2VPy/PVP/SCA, P2VPy/PVP/SBA and P2VPy/PVP/DDA ternary blends. The T_g values of these blends are tabulated in Tables 1–3. P2VPy is completely immiscible with PVP as shown by their widely separated glass transitions in their binary blends [31]. The addition of a sufficient amount of SBA or SCA gives rise to single T_gs of the ternary blends, while all P2VPy/PVP/DDA blends show two glass transitions even though DDA is saturated in the blends as evidenced by the melting peaks of DDA. Evidently, DDA is unable to miscibilize P2VPy and PVP blends. However, the single-T_g behavior of P2VPy/PVP/SBA and P2VPy/PVP/SCA blends is not a conclusive evidence of homogeneity state of the blends. As shown in Figs. 7 and 8, the T_gs of P2VPy and

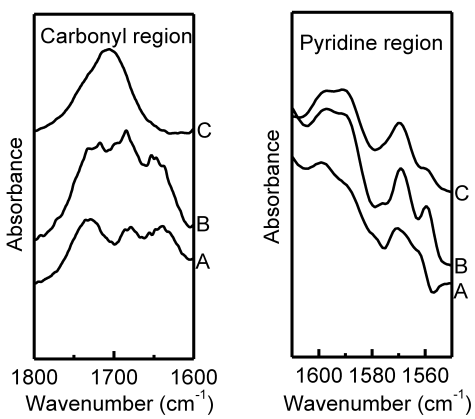

Fig. 9. FTIR spectra, recorded at 120 °C, in the carbonyl and pyridine regions of (A) $(P2VPy)_1(PVP)_1(SCA)_1$; (B) $(P2VPy)_1(PVP)_1(SBA)_1$ and (C) $(P2VPy)_1(PVP)_1(DDA)_1$ blends.

Table 1
T_gs of P2VPy/PVP/SCA ternary blends

Sample code	$(P2VPy)_x(PVP)_y(SCA)_z$, x:y:z	T_g (°C)	
A1	4:4:1	97	119
A2	2:2:1	90	
A3	1:1:1	55	
B1	1:3:0.5	101	117
B2	1:3:1	73	
B3	1:3:2	40	
C1	3:1:0.5	94	114
C2	3:1:1	84	
C3	3:1:2	57	

Table 2
T_gs of P2VPy/PVP/SBA ternary blends

Sample code	$(P2VPy)_x(PVP)_y(SBA)_z$, x:y:z	T_g (°C)	
A1	4:4:1	63	87
A2	2:2:1	39	
A3	1:1:1	2	
B1	1:3:0.5	55	
B2	1:3:1	45	
B3	1:3:2	14	
C1	3:1:0.5	73	
C2	3:1:1	36	
C3	3:1:2	9	

Table 3
T_gs of P2VPy/PVP/DDA ternary blends

Sample code	$(P2VPy)_x(PVP)_y(DDA)_z$, x:y:z	T_g (°C)	
A1	4:4:1	14	53
A2	2:2:1	25	58
A3	1:1:1	22	65

PVP approach each other at high acid contents. Therefore, the single-T_g behavior can be a result of simple overlap of two T_gs originated from separated P2VPy/acid and PVP/acid phases. Although the observed optical transparency of the single-T_g blends indicates that SCA or SBA can miscibilize P2VPy and PVP blends, further experimental evidence is needed to ascertain the miscibility of the single-T_g blends.

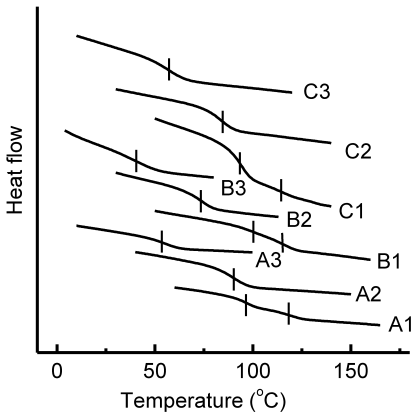

Fig. 10. DSC curves of P2VPy/PVP/SCA ternary blends (refer to Table 1 for sample code).

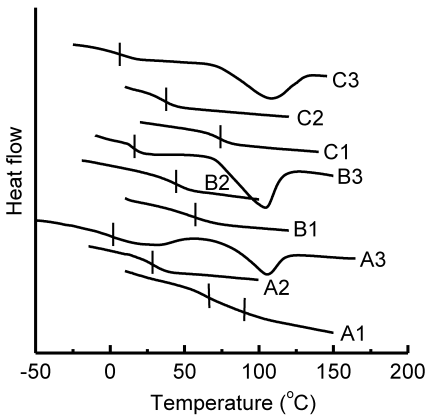

Fig. 11. DSC curves of P2VPy/PVP/SBA ternary blends (refer to Table 2 for sample code).

SEM was used to observe the phase structure. At a low SCA content, phase separation is still evident (Fig. 13). However, the single-T_g $(P2VPy)_2(PVP)_2(SCA)_1$ blend is homogeneous at low and high magnification. Similar results were also observed in P2VPy/PVP/SBA blends, and the micrographs are not shown here for brevity.

Solid-state NMR is a useful technique to study the miscibility of polymer blends [32]. When the domain size of a blend is below 30 nm, a single proton spin–lattice relaxation time, T_1(H), in the laboratory frame is observed, whereas a single proton spin–lattice relaxation time, $T_{1\rho}$(H), reveals an intimate mixing below the scale of 2–3 nm [32,40–43].

Based on the inversion-recovery mode for the experiment of the proton spin–lattice relaxation time in the laboratory frame, T_1(H) can be calculated using the following equation

$$\ln[(M_e - M_\tau)/(2M_e)] = -\tau/T_1(H)$$

where τ is the delay time used in the experiment and M_τ is the corresponding resonance intensity; M_e is the resonance intensity after complete recovery of the signals, which is

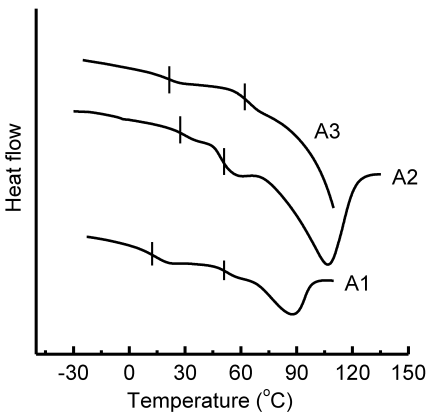

Fig. 12. DSC curves of P2VPy/PVP/DDA ternary blends (refer to Table 3 for sample code).

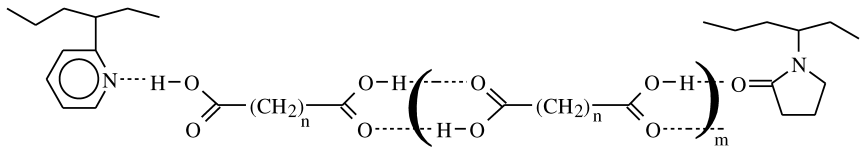

Scheme 2.

usually taken at $\tau \geq 5T_1(H)$. $T_1(H)$ is obtained from the slope of the plot of $\ln[(M_e - M_\tau)/(2M_e)]$ versus τ. Fig. 14 shows the $\ln[(M_e - M_\tau)/(2M_e)]$ versus τ plots of various single-T_g P2VPy/PVP/SCA blends based on the most intense resonance peak at 42 ppm at which both P2VPy and PVP have intensive resonance signals. All the blends show single $T_1(H)$s, demonstrating that the miscibility of the blends is below a scale of 20–30 nm. The single-T_g P2VPy/PVP/SBA blends also show single $T_1(H)$s, demonstrating their miscibility.

To investigate the miscibility at a smaller scale, proton spin–lattice relaxation behavior in the rotating frame was studied. In our previous study, a micro-heterogeneous P2VPy/PVP/BHPM blend exhibited a single $T_1(H)$ but a double-exponential decay behavior of $T_{1\rho}(H)$ [44]. The $T_{1\rho}(H)$ value is, according to spin-lock mode, calculated from

$$\ln(M_\tau/M_0) = -\tau/T_{1\rho}(H)$$

where τ is the delay time used in the experiment, and M_0 and M_τ are the intensities of a particular ^{13}C peak at zero time and at τ, respectively. Plots of $\ln(M_\tau/M_0)$ versus τ for the ternary P2VPy/PVP/SCA blends based on the resonance peak at 42 ppm are shown in Fig. 15. All the blends show single-exponential $T_{1\rho}(H)$ decay behavior, demonstrating miscibility at a scale of 2–3 nm. The P2VPy/PVP/SBA blends also show single-exponential $T_{1\rho}(H)$ decay behavior. It is surprising that P2VPy/PVP/SBA blends are miscible at such a scale even at quite a low SBA content.

Therefore, the single-T_g behavior of the blends is essentially a result of miscibilization rather than the overlap of two close T_gs. Thus miscibility is at a very small scale below 2 nm, which is almost at a molecular level. Therefore Scheme 1 is the more likely interaction. The ternary phase diagram can then be plotted based on the single T_g criteria (Fig. 16). Since DDA has poor solubility in the polymers, and P2VPy/PVP/DDA blends show immiscibility even at high DDA contents, it can be assumed that the miscibility region of this blend system, if any, is very small. The miscible region is then in the order P2VPy/PVP/SBA > P2VPy/PVP/SCA > P2VPy/PVP/DDA, and the miscibilization effect is in the order SBA > SCA > DDA.

It is apparent that miscibilization is promoted by specific interactions of the carboxylic groups with P2VPy and PVP. P2VPy and PVP are completely immiscible and therefore their mixing is endothermic and is unfavorable. The

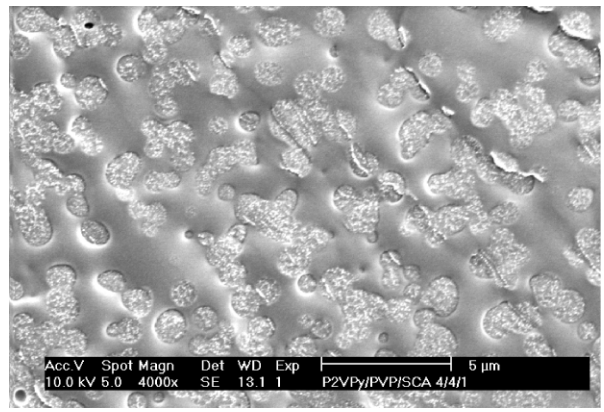

Fig. 13. SEM photomicrographs of $(P2VPy)_4(PVP)_4(SCA)_1$, 4000 × .

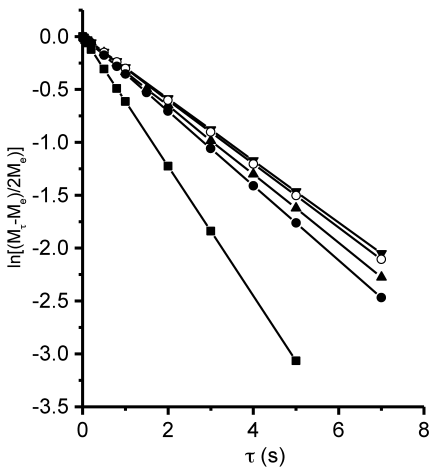

Fig. 14. $\ln[(M_e - M_\tau)/(2M_e)]$ versus τ plots of (▼) $(P2VPy)_2(PVP)_2(SCA)_1$; (○) $(P2VPy)_1(PVP)_3(SCA)_1$; (▲) $(P2VPy)_3(PVP)_1(SCA)_1$; (●) P2VPy and (■) PVP.

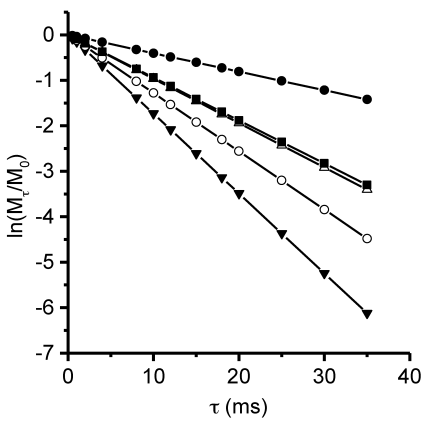

Fig. 15. $\ln(M_\tau/M_0)$ versus τ plots of (▼) $(P2VPy)_1(PVP)_3(SCA)_1$; (○) $(P2VPy)_2(PVP)_2(SCA)_1$; (△) $(P2VPy)_3(PVP)_1(SCA)_1$; (●) PVP and (■) P2VPy.

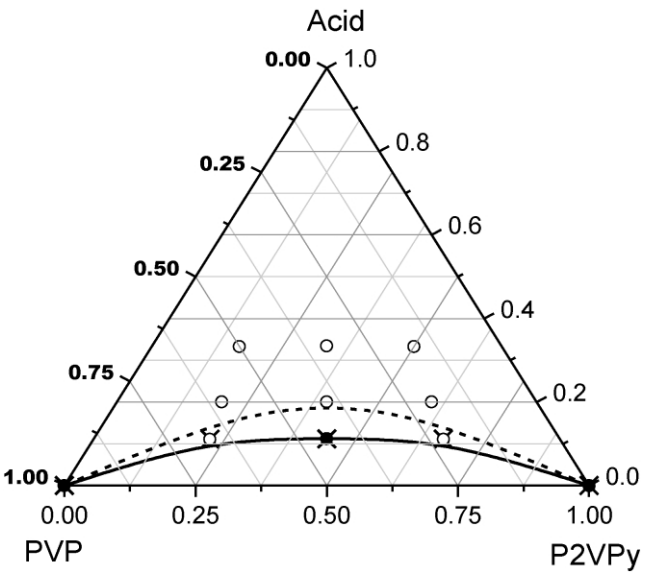

Fig. 16. Ternary phase diagram of P2VPy/PVP/acid blends. (○) miscible blends; (●) immiscible P2VPy/PVP/SBA blends and (×) immiscible P2VPy/PVP/SCA blends. Phase boundaries of P2VPy/PVP/SCA blends and P2VPy/PVP/SBA blends are represented by the dash line and solid line, respectively. Coordinate is in mole fraction.

exothermic interaction between the polymers and the carboxylic acid can offset the unfavorable endothermic mixing of P2VPy and PVP. When the number of specific interaction sites between the carboxylic groups and 2VPy and VP groups is large enough, the mixing of the ternary system becomes exothermic and the blends become miscible. DDA is saturated in the blends at a very low content thus there is not enough DDA in the amorphous P2VPy and PVP phase to interact with them to offset the unfavorable heat of mixing. However, although SCA interacts more strongly with P2VPy and PVP than SBA does, it is not as efficient as SBA to miscibilize P2VPy/PVP blend. This might be because SBA has a longer spacer. As shown in Scheme 1, SCA needs to bring P2VPy and PVP closer than SBA. Therefore it is more difficult for SCA to offset the unfavorable heat of mixing.

As compared to the P2VPy/PVP/bisphenol blends [27–29], the P2VPy/PVP/SCA and P2VPy/PVP/SBA blends have larger miscible regions. In other words, SCA and SBA are better miscibilizers than the bisphenols. The higher flexibility of SCA and SBA molecules as well as their higher acidity as compared to the bisphenols could be responsible for their better miscibilization effects.

4. Conclusion

The intensity of interaction of the dicarboxylic acids with P2VPy and PVP are in the order SCA > SBA > DDA. DDA has the lowest saturation content in P2VPy and PVP, and SCA has the highest saturation content. Both SBA and SCA are able to miscibilize P2VPy and PVP blend to a molecular level. Although SBA interacts with P2VPy and PVP not as strongly as SCA does, its longer flexible spacer between two carboxylic end groups facilitates the involvement of the two carboxylic groups in simultaneous interaction with P2VP and PVP, and thus it has a better miscibilization effect than SCA does. However, DDA, which has a longer spacer than SBA, is unable to miscibilize P2VPy and PVP blends. Since the non-polar spacer is not compatible with P2VPy and PVP, the long spacer results in a low saturation content. Therefore a longer spacer does not necessarily guarantee a better miscibilization effect.

References

[1] Brannock GR, Paul DR. Macromolecules 1990;23:5240.
[2] Kwei TK, Frisch JL, Radigan W, Vogel S. Macromolecules 1977;10:157.
[3] Shah VS, Keitz JD, Paul DR, Barlow JW. J Appl Polym Sci 1986;32:3863.
[4] Iruin JJ, Eguiazabal I, Guzman GM. Eur Polym J 1989;25:1169.
[5] Pomposo JA, Calahorra E, Eguiazabal I, Cortazar M. Macromolecules 1993;26:2104.
[6] Min KE, Chiou JS, Barlow JW, Paul DR. Polymer 1987;28:1721.
[7] Woo EM, Tseng YC. Macromol Chem Phys 2000;201:1877.
[8] Guo Q. Eur Polym J 1996;32:1409.
[9] Goh SH, Ni X. Polymer 1999;40:5733.
[10] Manestrel CL, Bhagwagar DE, Painter PC, Coleman MM, Graf JF. Macromolecules 1992;25:7101.
[11] Hong BK, Kim JY, Jo WH, Lee SC. Polymer 1997;38:4373.
[12] Kuo SW, Lin CL, Chang FC. Macromolecules 2002;35:278.
[13] Jo WH, Kwon YK, Kwon IH. Macromolecules 1991;24:4708.
[14] Lehn JM. Angew Chem Int Ed Engl 1990;29:1304.
[15] Ruokolainen J, Tanner J, Ikkala O, ten Brinke G, Thomas EL. Macromolecules 1998;31:3532.
[16] He Y, Asakawa N, Inoue Y. J Polym Sci, Part B: Polym Phys 2000;38:1848.
[17] He Y, Asakawa N, Inoue Y. J Polym Sci, Part B: Polym Phys 2000;38:2891.
[18] He Y, Asakawa N, Inoue Y. Macromol Chem Phys 2001;202:1035.
[19] Li J, He Y, Ishida K, Yamane T, Inoue Y. Polym J 2001;33:773.
[20] Li J, He Y, Inoue Y. J Polym Sci, Part B: Polym Phys 2001;39:2108.
[21] He Y, Asakawa N, Li J, Inoue Y. J Appl Polym Sci 2001;82:640.
[22] Watanabe T, He Y, Asakawa N, Yoshie N, Inoue Y. Polym Int 2001;50:463.
[23] Wu C, Akiyama S, Mabuchi T, Nitta K. Polym J 2001;33:792.
[24] Wu C, Yamagishi T, Nakamoto Y, Ishida S, Nitta K, Kubota S. J Polym Sci, Part B: Polym Phys 2000;38:2285.
[25] Wu C, Otani Y, Namiki N, Emi H, Nitta K, Kubota S. J Appl Polym Sci 2001;82:1788.
[26] Wu C. J Appl Polym Sci 2001;80:2468.
[27] Li XD, Goh SH. J Polym Sci, Part B: Polym Phys 2001;39:1815.
[28] Li XD, Goh SH. J Polym Sci, Part B: Polym Phys 2002;40:1125.
[29] Li XD, Goh SH. J Appl Polym Sci 2002; in press.
[30] Kuo SW, Chan SC, Chang FC. Polymer 2002;43:3653.
[31] Li XD, Goh SH. J Appl Polym Sci 2001;81:901.
[32] McBrierty VJ, Packer KJ. Nuclear magnetic resonance in solid polymers. Cambridge, NY: Cambridge University Press; 1993.
[33] Coleman MM, Graf JF, Painter PC. Specific interaction and miscibility of polymer blends. Lancaster, PA: Technomic; 1991.
[34] Lee JY, Painter PC, Coleman MM. Macromolecules 1988;21:954.
[35] Cesteros LC, Meaurio E, Katime I. Macromolecules 1993;26:2323.

[36] Drago RS, O'Bryan N, Vogel GC. J Am Chem Soc 1969;91:2883.
[37] Drago RS, Epley TD. J Am Chem Soc 1970;92:3924.
[38] Lee JY, Painter PC, Coleman MM. Macromolecules 1988;21:346.
[39] Luo XF, Goh SH, Lee SY. Macromol Chem Phys 1999;200:399.
[40] Schantz S, Ljungqvist N. Macromolecules 1993;26:6517.
[41] Geppi M, Forte C, Passaglia E, Mendez B. Macromol Chem Phys 1998;199:1957.
[42] Guo M. Trend Polym Sci 1996;4:238.
[43] Yi JZ, Goh SH. Polymer 2001;42:9313.
[44] Li XD, Goh SH. In preparation.